Supporting Information

Atomically dispersed ruthenium sites with electron-rich environments in intermetallic compounds for high-current-density hydrogen evolution

Huaifang Zhang[a, b‡], Chuanqi Cheng[c‡], Jin Zhou[d‡], Chaoqun Ma[a, b], Peidong Shi[e], Haoming Wu[a, b], Pengfei Yin[c], Wenbin Cao[a], Jing Xia[f], Lijie Zhu[g*], An-Liang Wang[e*], Qipeng Lu[a, b, h*]

[a] School of Materials Science and Engineering, University of Science and Technology Beijing, Beijing 100083, China. E-mail: qipeng@ustb.edu.cn

[b] Shunde Innovation School, University of Science and Technology Beijing, Foshan 528399, China

[c] Institute of New Energy Materials, School of Materials Science and Engineering, Tianjin University, Tianjin 300072, China

[d] School of Chemical Engineering and Technology, Tianjin University, Tianjin 300072, China

[e] School of Chemistry and Chemical Engineering, Shandong University, Jinan 250100, China. E-mail: alwang@sdu.edu.cn

[f] Key Laboratory of Photochemical Conversion and Optoelectronic Materials, Technical Institute of Physics and Chemistry, Chinese Academy of Sciences, Beijing 100190, China

[g] School of Instrument Science and Opto-Electronics Engineering, Beijing Information Science and Technology University, Beijing 100192, China. E-mail: ljzhu@bistu.edu.cn

[h] Zhongguancun Institute of Human Settlements Engineering and Materials, Beijing 100083, China

‡These authors contributed equally to this work.

Experimental

Reagents and chemicals

Graphene oxide (GO) was purchased from Nanjing XFNANO Materials Tech Co., Ltd (Nanjing, China). Sodium nitrate ($NaNO_3$, 99.0%) and poly (vinyl alcohol) (PVA, *Mw* = 1750 ± 50) were obtained from Sinopharm Chemical Reagent Co., Ltd (Shanghai, China). Ruthenium nitrosyl nitrate solution ($Ru(NO)(NO_3)_3$, 1.5%) and gallium nitrate nonahydrate ($Ga(NO_3)_3 \cdot xH_2O$, 99.99%) were supplied by Macklin Biochemical Co., Ltd (Shanghai, China). All reagents and chemicals were of analytical grade and used without further purification.

Synthesis of RuGa/N-rGO, Ru/N-rGO and N-rGO

In a standard synthesis of RuGa/N-rGO, 0.075 mmol $Ru(NO)(NO_3)_3$ and 0.075 mmol $Ga(NO_3)_3 \cdot 9H_2O$ were added to 0.5 mL of PVA aqueous solution (20 mg mL^{-1}) and sonicated until completely dissolved. Meanwhile, 64 mg of GO was dissolved in 4 mL of deionized water and continuously sonicated to form a homogeneous solution. Then, GO aqueous solution was quickly added to the above PVA solution. The mixture was strongly shaken to form the $Ru(NO)(NO_3)_3$-$Ga(NO_3)_3$/GO-PVA hydrogels. Subsequently, the resulting hydrogels were freeze-dried at -50 °C to form the $Ru(NO)(NO_3)_3$-$Ga(NO_3)_3$/GO-PVA aerogels. Finally, the aerogels were annealed at different annealing temperatures for 12 hours under H_2/Ar (10 vol.% H_2) with a heating rate of 5 ^{o}C min^{-1}. The aerogels annealed at 700, 800, and 900 ^{o}C were designated as RuGa/N-rGO-1, RuGa/N-rGO-2, and RuGa/N-rGO-3, respectively. The final products

were washed with deionized water several times.

The synthetic procedures of Ru/N-rGO were similar to those of RuGa/N-rGO-2 without the addition of $Ga(NO_3)_3 \cdot 9H_2O$.

The synthetic procedures of N-rGO were similar to those of RuGa/N-rGO-2, but 0.525 mmol of $NaNO_3$ was used instead of the 0.075 mmol of $Ru(NO)(NO_3)_3$ and 0.075 mmol of $Ga(NO_3)_3 \cdot 9H_2O$.

Physicochemical characterizations

The X-ray powder diffraction (XRD) patterns of different nanomaterials were taken on a Bruker D8 Advance diffractometer equipped with Cu Kα radiation (λ = 0.15406 nm). The scanning electron microscopy (SEM) images were collected on a Hitachi S-4800 scanning electron microscope. Transmission electron microscopy (TEM) images, high-resolution TEM (HRTEM) images, and selected area electron diffraction (SAED) patterns were obtained on a JEOL JEM-2100F transmission electron microscope manipulated at 200 kV. High-angle annular dark-field scanning transmission electron microscopy (HAADF-STEM) images, aberration-corrected HAADF-STEM images, and energy-dispersive X-ray spectroscopy (EDX) elemental mapping images were performed on a JEOL JEM-ARM300F Grand ARM transmission electron microscope operated at an accelerating voltage of 300 kV accelerating voltage with a cold field-emission electron gun, double spherical aberration correctors, and SDD-type EDX detectors. Atomic force microscopy (AFM) images were achieved by using a Bruker Dimension Icon atomic force microscope. The Raman spectra were recorded on a

Horiba Jobin Yvon LabRam HR800 spectrometer employing a 514 nm laser light. The X-ray photoelectron spectroscopy (XPS) spectra were carried out on a Thermo Scientific ESCALAB 250Xi spectrometer using an Al Kα radiation, and all binding energies were calibrated by the C 1s peak energy of 284.8 eV. The Brunauer-Emmett-Teller (BET) specific surface area and pore size were carried out on a Micromeritics ASAP 2460 Surface Area and Porosimetry analyzer at 77 K. The accurate metal contents were quantified by inductively coupled plasma atomic emission spectroscopy (ICP-AES) on an Agilent ICPOES730 instrument.

Electrochemical measurements

All electrochemical measurements were performed on a CHI 760D electrochemical workstation (Shanghai, Chenhua Co.) with a standard three-electrode system. For a conventional three-electrode system, a catalyst-modified glassy carbon electrode (GCE, 0.0706 cm^2) served as the working electrode, a graphite rod was regarded as the assistant electrode, and a saturated calomel electrode (SCE) was used as the reference electrode, respectively. For the preparation of the working electrode, different amount of the as-prepared catalysts was uniformly dispersed in 1.0 mL of isopropanol to prepare the homogeneous catalyst ink. Subsequently, the 15 μL of homogeneous catalyst ink was pipetted onto the surface of cleaned GCE and dried at room temperature. Finally, 3.0 μL of Nafion solution (0.5 wt.%) was dropped onto the surface of the catalyst-modified working electrode. The loading amount of metal (Ru or Pt) on the working electrode was controlled to be 6.0 μg.

The N_2-saturated 0.5 M H_2SO_4 and 1.0 M KOH solutions were used as the acidic and alkaline electrolytes, respectively. All the potential values presented in this paper have been calibrated to the reversible hydrogen electrode (RHE) using the conversion formula: $E_{RHE} = E_{SCE} + 0.0591\ pH + 0.242$. The linear sweep voltammetry (LSV) measurements were assessed with a sweep rate of 5 mV s^{-1} and all data were manually *iR*-corrected. The linear regions of the Tafel plots were fitted by the Tafel equation $\eta = a + b\log|j|$, where η stands for the overpotential, a, b and j refer to the Tafel constant, Tafel slope, and the current density, respectively. The double-layer capacitance (C_{dl}) of the different electrocatalysts was obtained from the cyclic voltammogram (CV) measurements at various scan rates of 20~200 mV s^{-1} in a non-faradic potential range of 0.1 V to 0.2 V. The value of C_{dl} was calculated by fitting the difference between the positive and negative current densities (Δj) at 0.15 V against the scan rate, where the slope is twice C_{dl}. The electrochemical impedance spectroscopy (EIS) measurements were investigated with a frequency range from 100 kHz to 0.01 Hz. The accelerated degradation tests were measured for 10,000 cycles from -0.2 to 0.0 V with a sweep rate of 100 mV s^{-1}.

Calculation details

Density functional theory (DFT) calculations were performed using Vienna *ab-initio* Simulation Package (VASP) software.[1, 2] The projector augmented wave (PAW) pseudopotential with the Perdew-Burke-Ernzerhof (PBE) and generalized gradient approximation (GGA) exchange-correlation function was employed in the computations.[3-5] The DFT-D3 method was adopted to describe the van der Waals

interactions.[6, 7] The cutoff energy of 500 eV was employed for the plane-wave basis set of all calculations, and a Monkhorst-Pack k-point mesh of 3×3×1 was used in the structural optimization. The convergence threshold in structural optimization was set as 10^{-5} eV for energy and 0.01 eV $Å^{-1}$ for force. The transition state (TS) searches are performed using the Dimer method in the VTST package. The final force on each atom was < 0.2 eV $Å^{-1}$. The TS searches are conducted by using the climbing-image nudged elastic band (CI-NEB) method to generate initial guess geometries, followed by the dimer method to converge to the saddle points. To avoid periodical interactions, a vacuum space of 15 Å was added in the z-direction. The RuGa (110), Pt (111), and Ru (001) facets are chosen as the structural models for DFT calculations. The Gibbs free energy change (ΔG) of each elementary reaction can be computed by the following equation: $\Delta G = \Delta E + \Delta ZPE - T\Delta S$.

Where ΔE is the reaction energy difference, ΔZPE is the zero-point energy change, T is the temperature, and ΔS is the entropy change, respectively.

Figures and Tables

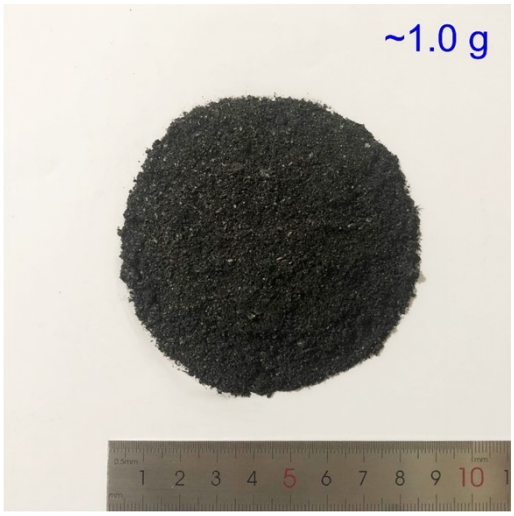

Figure S1. Photograph of RuGa/N-rGO electrocatalyst (~1.0 g).

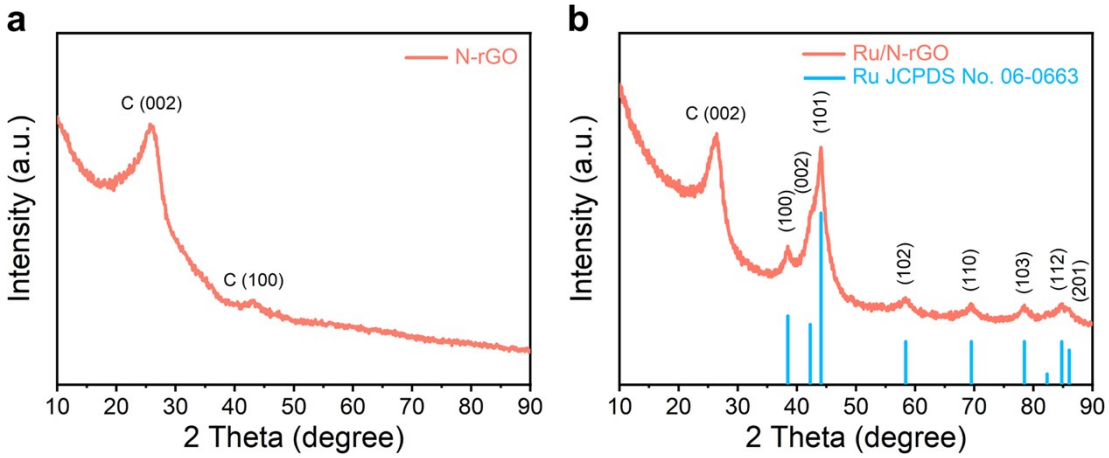

Figure S2. XRD patterns of (a) N-rGO and (b) Ru/N-rGO.

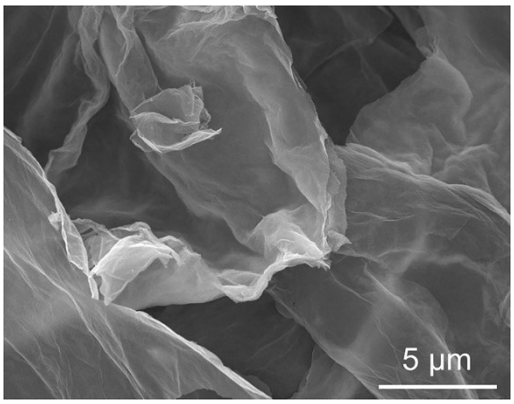

Figure S3. SEM image of RuGa/N-rGO.

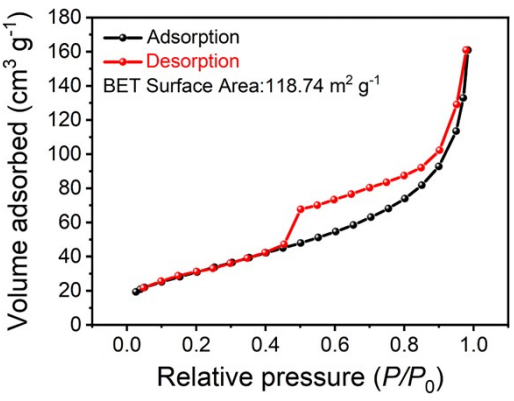

Figure S4. N_2 adsorption-desorption isotherms of RuGa/N-rGO.

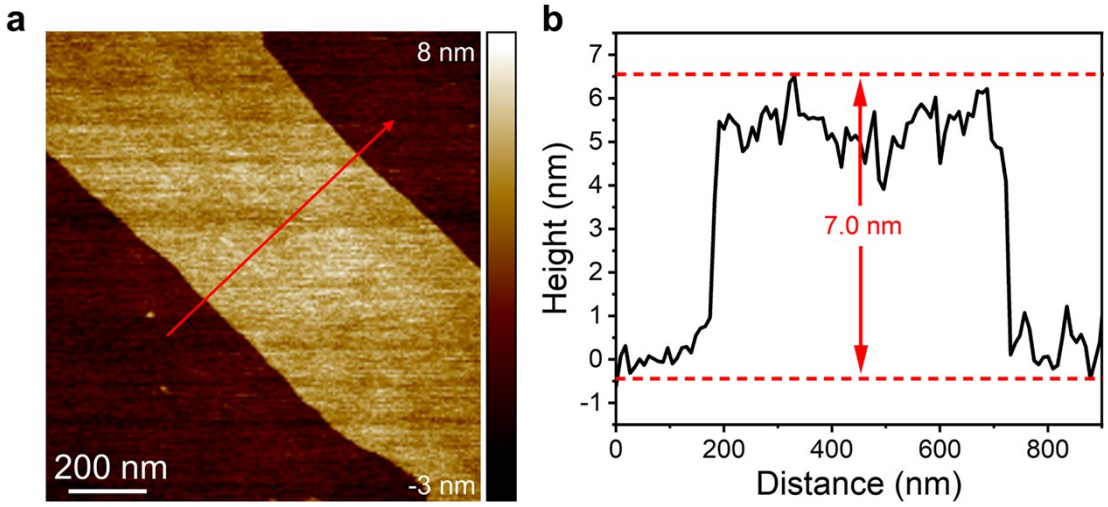

Figure S5. (a) AFM image of RuGa/N-rGO. (b) The corresponding height profile along the red line in a.

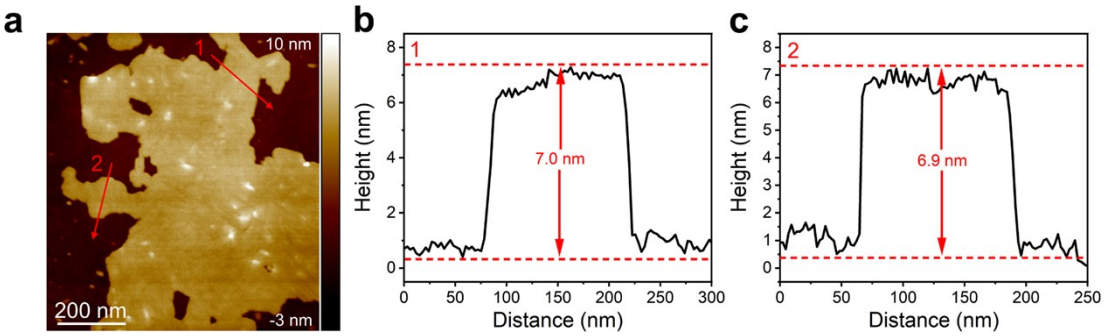

Figure S6. (a) AFM image of Ru/N-rGO. (b,c) The corresponding height profiles along the red lines in a.

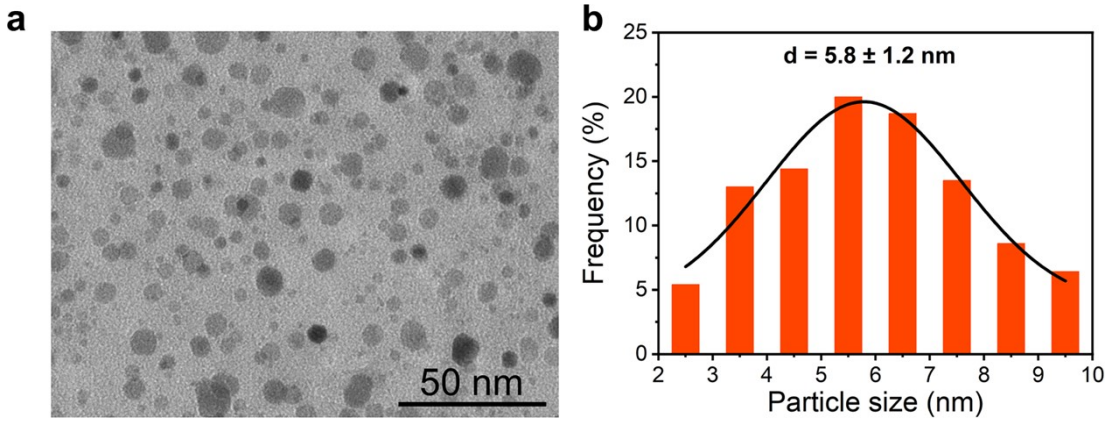

Figure S7. (a) TEM image of Ru/N-rGO. (b) The corresponding particle size distribution histogram.

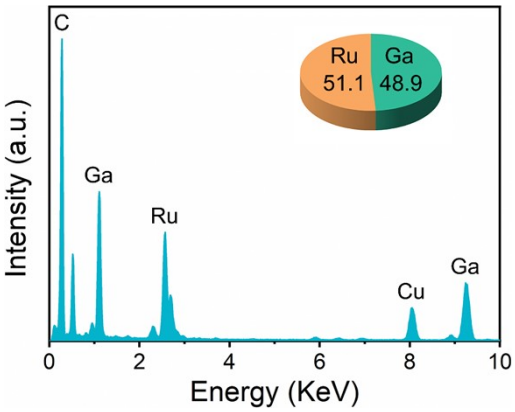

Figure S8. EDX spectrum of RuGa/N-rGO.

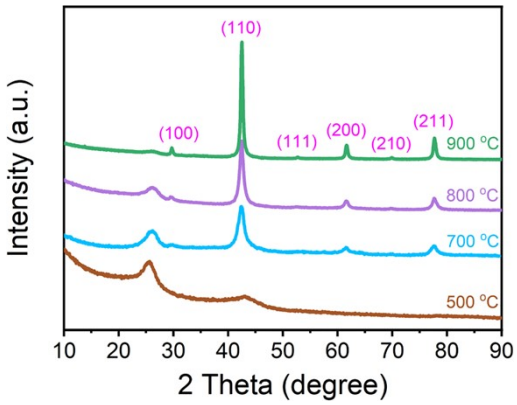

Figure S9. XRD patterns of RuGa/N-rGO samples annealed at different temperatures for 12 h.

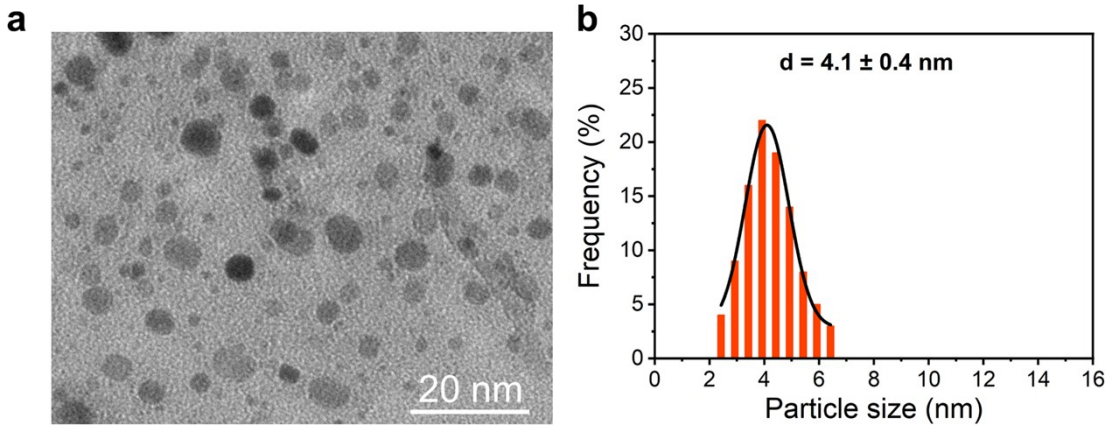

Figure S10. (a) TEM image of RuGa/N-rGO-1. (b) The corresponding particle size distribution histogram.

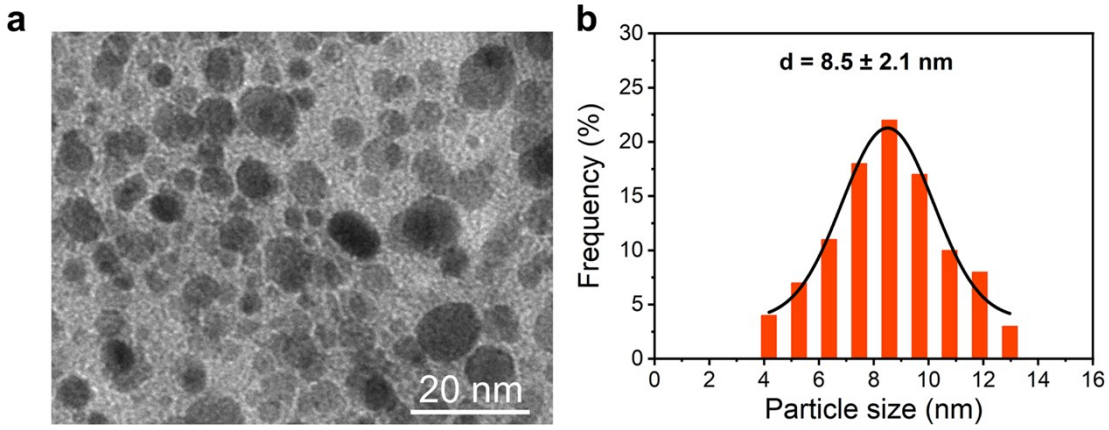

Figure S11. (a) TEM image of RuGa/N-rGO-3. (b) The corresponding particle size distribution histogram.

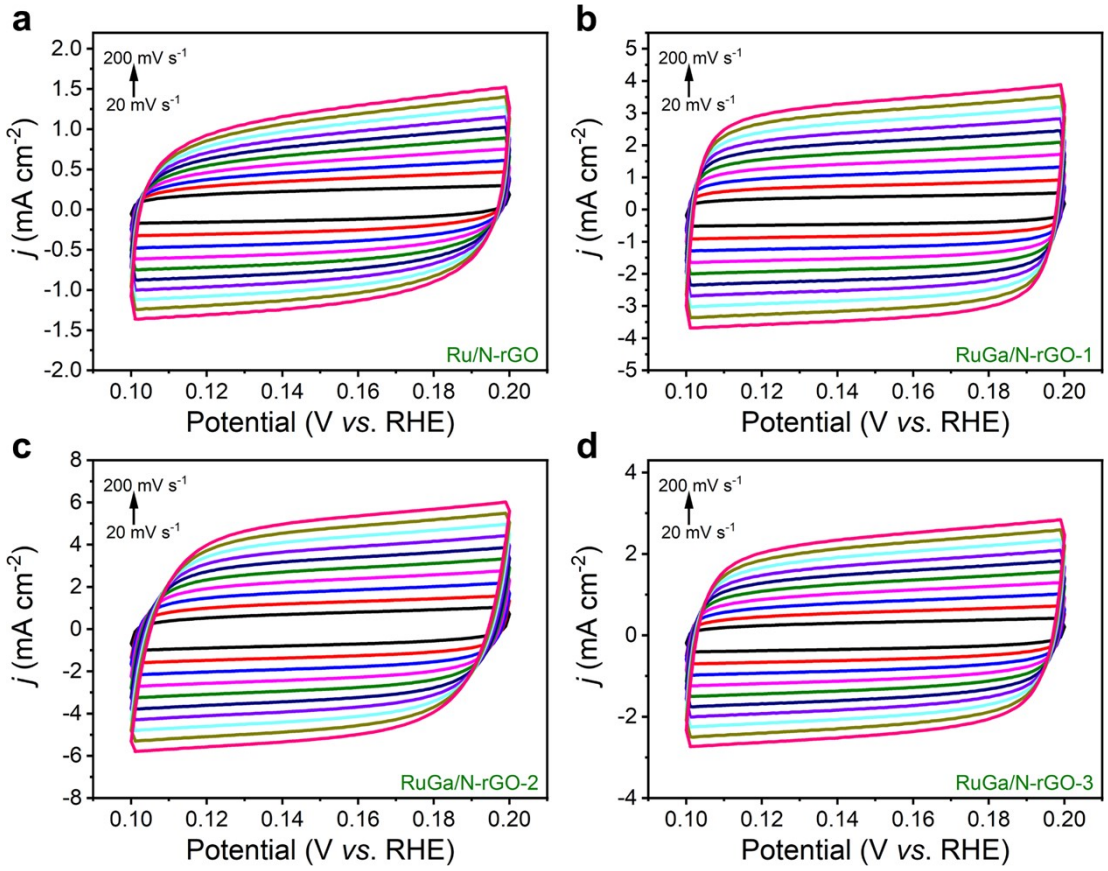

Figure S12. Cyclic voltammetry curves of (a) Ru/N-rGO, (b) RuGa/N-rGO-1, (c) RuGa/N-rGO-2, and (d) RuGa/N-rGO-3 at different scan rates in 0.5 M H_2SO_4 solution.

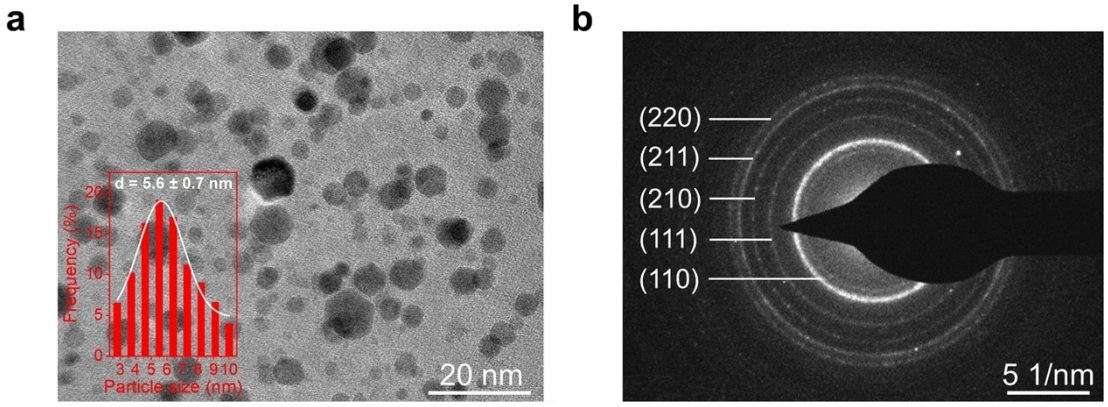

Figure S13. (a) Low-magnification TEM image of RuGa/N-rGO-2 after the long-term durability test in 0.5 M H_2SO_4 solution, the inset is the corresponding size distribution histogram. (b) SAED pattern of RuGa/N-rGO-2 after the long-term durability test in 0.5 M H_2SO_4 solution.

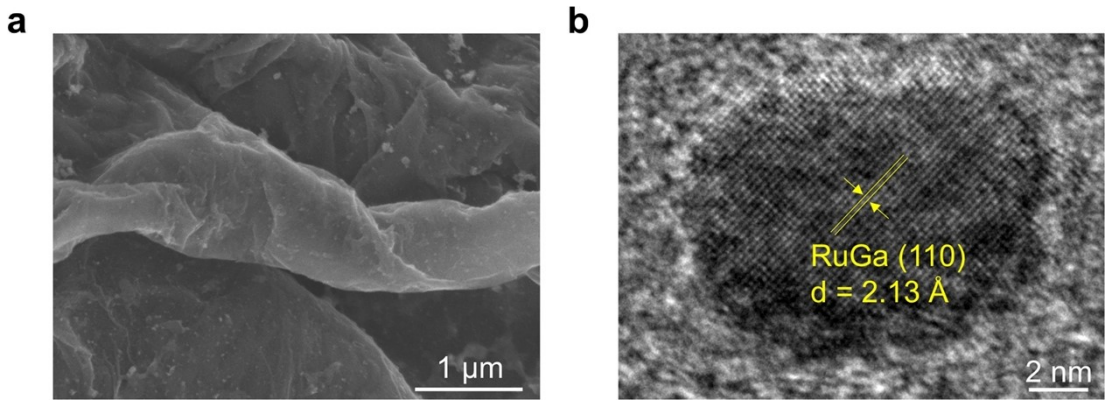

Figure S14. (a) SEM image and (b) HRTEM image of RuGa/N-rGO-2 after the long-term durability test in 0.5 M H_2SO_4 solution.

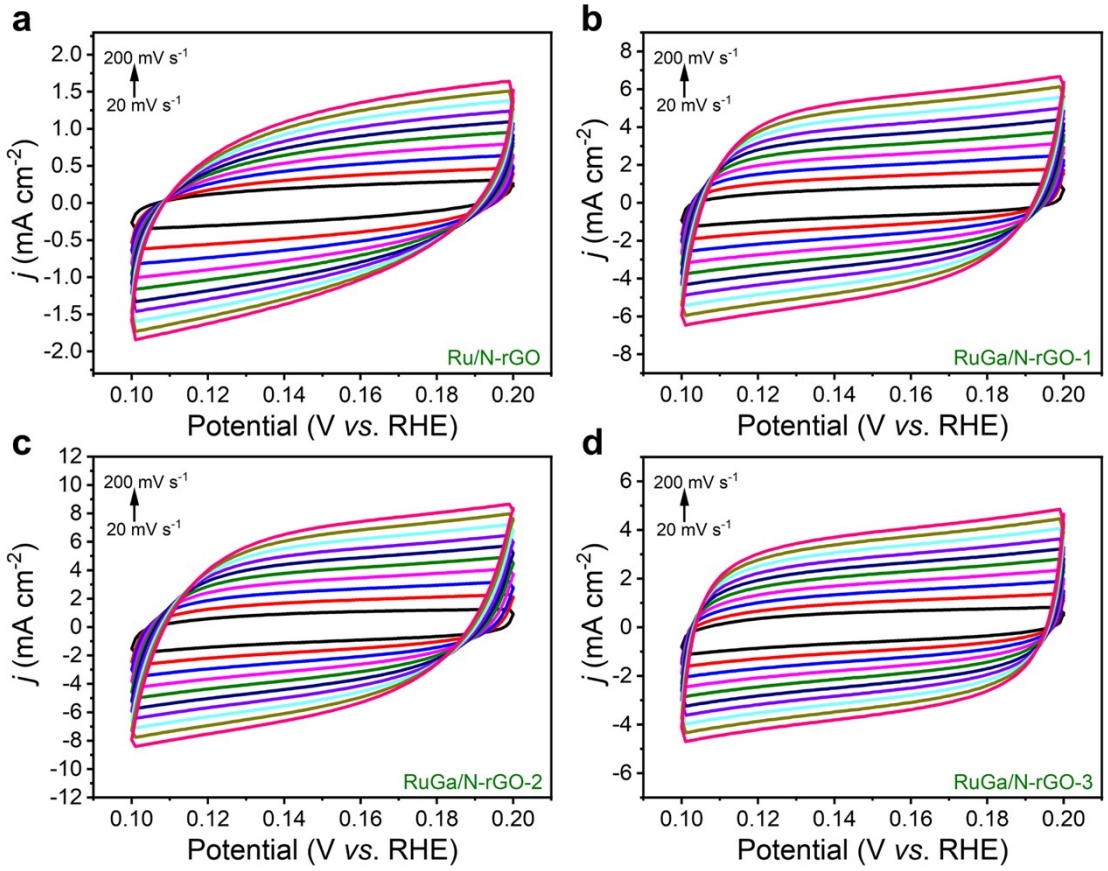

Figure S15. Cyclic voltammetry curves of (a) Ru/N-rGO, (b) RuGa/N-rGO-1, (c) RuGa/N-rGO-2, and (d) RuGa/N-rGO-3 at different scan rates in 1.0 M KOH solution.

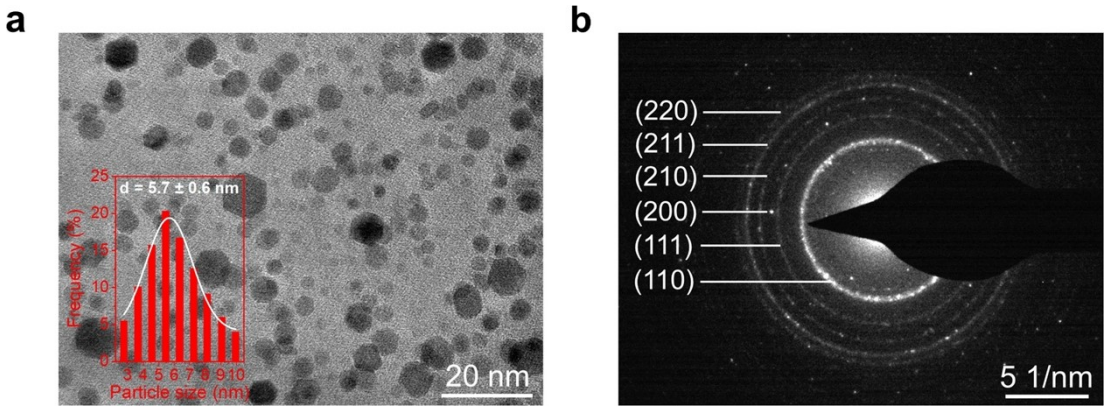

Figure S16. (a) Low-magnification TEM image of RuGa/N-rGO-2 after the long-term durability test in 1.0 M KOH solution, the inset is the corresponding size distribution histogram. (b) SAED pattern of RuGa/N-rGO-2 after the long-term durability test in 1.0 M KOH solution.

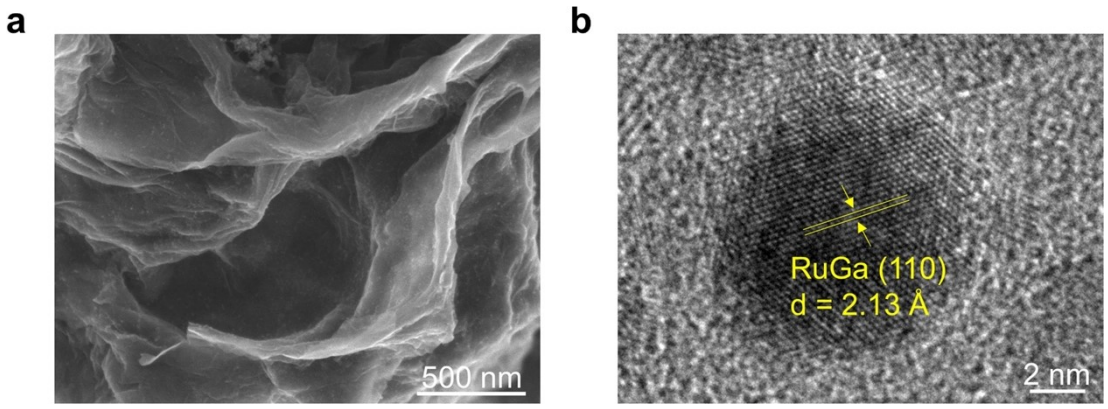

Figure S17. (a) SEM image and (b) HRTEM image of RuGa/N-rGO-2 after the long-term durability test in 1.0 M KOH solution.

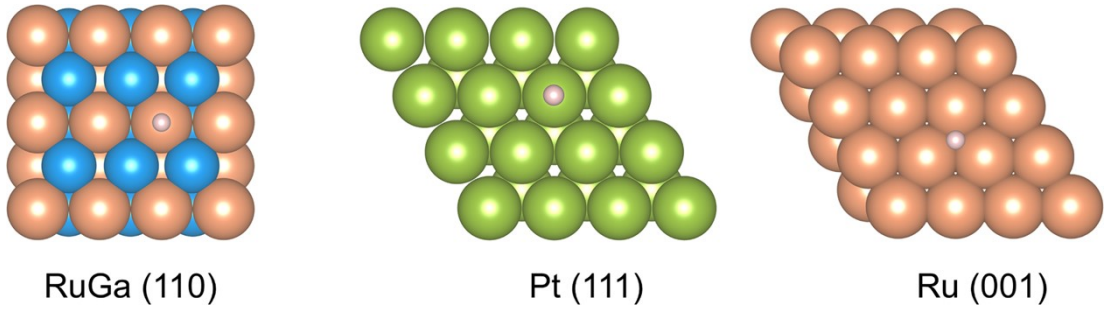

Figure S18. Structural models of *H intermediate for the acidic HER process on RuGa (110), Pt (111), and Ru (001).

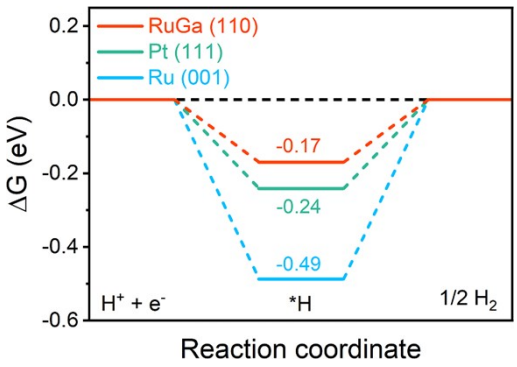

Figure S19. Calculated free energy diagrams for HER on RuGa (110), Pt (111), and Ru (001) in acidic condition.

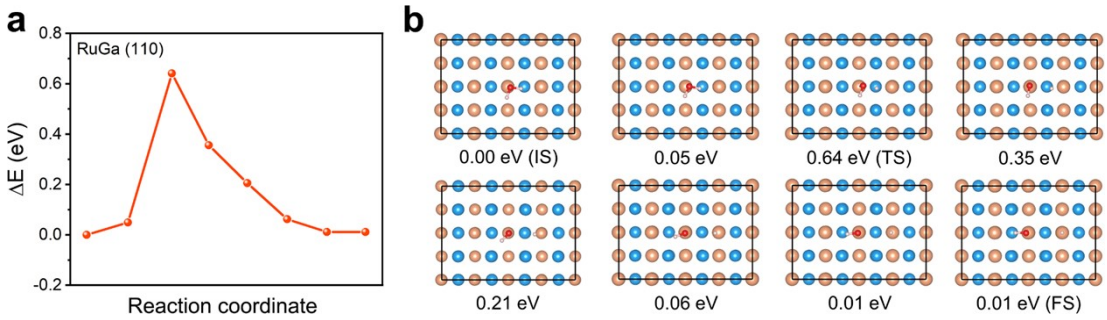

Figure S20. (a) Predicted water dissociation energy barriers on RuGa (110) and (b) corresponding structural models.

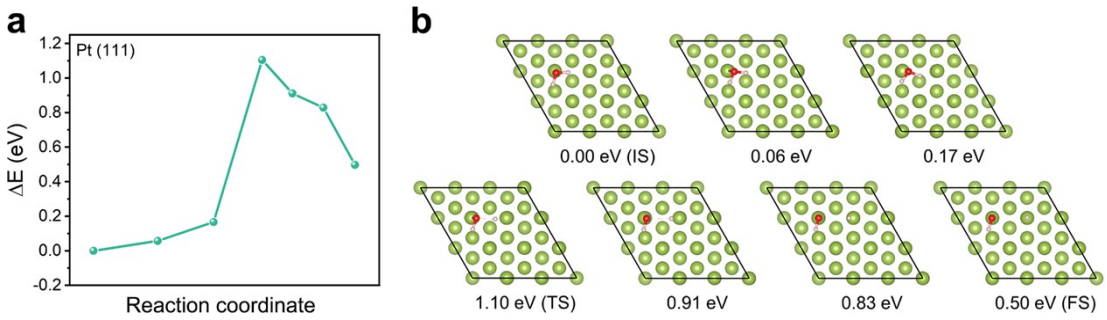

Figure S21. (a) Predicted water dissociation energy barriers on Pt (111) and (b) corresponding structural models.

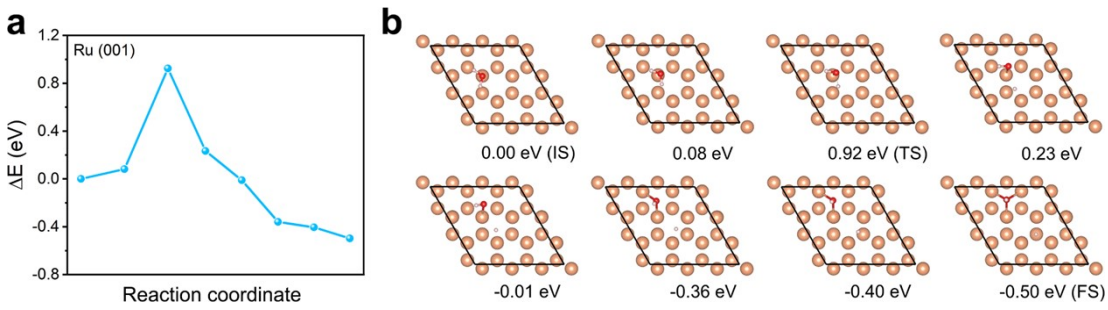

Figure S22. (a) Predicted water dissociation energy barriers on Ru (001) and (b) corresponding structural models.

Table S1. Mass and atomic percentage of Ru and Ga elements obtained from ICP-AES.

Catalysts	Ru (wt.%)	Ga (wt.%)	Ru/Ga (at.%)
RuGa/N-rGO-1	16.86	11.58	50.11:49.89
RuGa/N-rGO-2	18.37	12.60	50.14:49.86
RuGa/N-rGO-3	17.52	12.01	50.16:49.84
Ru/N-rGO	16.40	N/A	N/A

Table S2. Comparison of the HER performance of the RuGa/N-rGO-2 with some recently reported Ru-based catalysts in 0.5 M H_2SO_4 solution.

Catalysts	Overpotential at 10 mA cm^{-2} (mV)	Tafel slope ($mV\ dec^{-1}$)	References
RuGa/N-rGO-2	**32**	**29.0**	**This work**
Ru-Cu-2	34	48	*Nano Energy*, 2022, **92**, 106763
RuP_2@NPC	38	38	*Angew. Chem. Int. Ed.*, 2017, **56**, 11559
Ru_2B_3@BNC	41	60.7	*Nano Energy*, 2020, **75**, 104881
Co-SAC/RuO_2	45	58	*Angew. Chem. Int. Ed.*, 2022, **61**, e202114951
Ru/RuS_2-2	45	24.4	*Angew. Chem. Int. Ed.*, 2021, **60**, 12328
Pd@Ru (111) Ths	48	51	*ACS Nano*, 2021, **15**, 5178
Ru_1CoP/CDs-1000	49	51.6	*Angew. Chem. Int. Ed.*, 2021, **60**, 7234
NiRu@N-C	50	36	*J. Mater. Chem. A*, 2018, **6**, 1376
Ni@Ni_2P-Ru HNRs	51	35	*J. Am. Chem. Soc.*, 2018, **140**, 2731
RuB_2	52	66.9	*ACS Energy Lett.*, 2020, **5**, 2909
Ru@Co-SAs/N-C	57	55	*Nano Energy*, 2019, **59**, 472
RuNi/CQDs	58	55	*Angew. Chem. Int. Ed.*, 2020, **59**, 1718
Ru-HPC	61.6	66.8	*Nano Energy*, 2019, **58**, 1
Ru-RuO_2@NPC	68	56	*Appl. Catal. B.*, 2022, **302**, 120838
CuPor-RuN_3	73	73	*Adv. Funct. Mater.*, 2021, **31**, 2107290
RuP_2@PC	77.2	41.2	*J. Mater. Chem. A*, 2021, **9**, 12276
2.20wt% Ru Sas-Ni_2P	125	71	*Nano Energy*, 2021, **80**, 105467
Cu_{2-x}S@Ru NPs	129	51	*Small*, 2017, **13**, 1700052

Table S3. Comparison of the HER performance of the RuGa/N-rGO-2 with some recently reported Ru-based catalysts in 1.0 M KOH solution.

Catalysts	Overpotential at 10 mA cm^{-2} (mV)	Tafel slope ($mV\ dec^{-1}$)	References
RuGa/N-rGO-2	**20**	**28.2**	**This work**
RuO_2@C	20	46	*Nano Energy*, 2019, **55**, 49
RuO_2/NiO/NF	22	31.7	*Small*, 2018, **14**, 1704073
RuCoP	23	37	*Energy Environ. Sci.*, 2018, **11**, 1819
4H/fcc Ru NTs	23	29.4	*Small*, 2018, **14**, 1801090
Ru2-GC	25	65	*ACS Catal.*, 2018, **8**, 11094
Ru@NC	26	36	*Angew. Chem. Int. Ed.*, 2018, **57**, 5848
RuCo@NC	28	31	*Nat. Commun.*, 2017, **8**, 14969
Ni@Ni_2P-Ru HNRs	31	41	*J. Am. Chem. Soc.*, 2018, **140**, 2731
Ru@CN-0.16	32	53	*Energy Environ. Sci.*, 2018, **11**, 800
Ru/TiO_2	32	60	*Nano Energy*, 2021, **88**, 106211
NiRu@N-C	32	64	*J. Mater. Chem. A*, 2018, 6, 1376
Ru-Cu-2	33	37	*Nano Energy*, 2022, **92**, 106763
Ru-Ru_2P@PC	43.4	35.1	*J. Mater. Chem. A*, 2019, **7**, 5621
RuP_2@NPC	52	69	*Angew. Chem. Int. Ed.*, 2017, **56**, 11559
Ru@CNT	63	76	*Nat. Commun.*, 2021, **12**, 4018
RuP_2@PC	78.9	36.7	*J. Mater. Chem. A*, 2021, **9**, 12276
Ru-RuO_2@NPC	79	73	*Appl. Catal. B.*, 2022, **302**, 120838
$Cu_{2-X}S$@Ru NPS	82	48	*Small*, 2017, **13**, 1700052

Table S4. Comparison of the HER performance of the RuGa/N-rGO-2 with some recently reported electrocatalysts in 1.0 M KOH solution.

Catalysts	Overpotential at 500 mA cm^{-2} (mV)	Overpotential at 1000 mA cm^{-2} (mV)	References
RuGa/N-rGO-2	**105**	**156**	**This work**
$MoNi_4/MoO_{3-x}$	114	156	*Adv. Mater.*, 2017, **29**, 1703311
FeIr/NF	125	204	*Appl. Catal. B.*, 2020, **278**, 119327
Ru-CoO_x/NF	~170	252	*Small*, 2021, **17**, 2102777
$NiMoO_x$/NiMoS	174	236	*Nat. Commun.*, 2020, **11**, 5462
MoS_2/Mo_2C	191	220	*Nat. Commun.*, 2019, **10**, 269
Co-Mo_5N_6	~200	280	*Adv. Energy. Mater.*, 2020 **10**, 2002176
Ni_3S_2/Cr_2S_3@NF	~210	227	*J. Am. Chem. Soc.* 2022, **144**, 6028
P-Fe_3O_4/IF	~210	~240	*Adv. Mater.*, 2019, **31**, 1905107
FeP/Ni_2P	~220	~265	*Nat. Commun.*, 2018, **9**, 2551
Ni_2P/NF	~230	306	*J. Am. Chem. Soc.*, 2019, **141**, 7537
$Ni_{2(1-x)}Mo_{2x}P$	240	294	*Nano Energy*, 2018, **53,** 492
Ni_3N/Pt nanosheets	~270	~440	*Adv. Energy Mater.* 2017, **7**, 1601390
HC-MoS_2/Mo_2C	~390	441	*Nat. Commun.*, 2020, **11**, 3724
NC/Ni_3Mo_3N/NF	~400	~680	*Appl. Catal. B.*, 2020, **272**, 118956
IrFe/NC	~430	850	*Appl. Catal. B.*, 2019, **258**, 117965

References

1 G. Kresse and J. Furthmüller, *Phys. Rev. B*, 1996, **54**, 11169-11186.

2 G. Kresse and J. Hafner, *Phys. Rev. B*, 1993, **47**, 558-561.

3 P. E. Blöchl, *Phys. Rev. B*, 1994, **50**, 17953-17979.

4 B. Hammer, L. B. Hansen and J. K. Nørskov, *Phys. Rev. B*, 1999, **59**, 7413-7421.

5 J. P. Perdew, K. Burke and M. Ernzerhof, *Phys. Rev. Lett.*, 1996, **77**, 3865-3868.

6 J. Klimeš, D. R. Bowler and A. Michaelides, *Phys. Rev. B*, 2011, **83**, 195131.

7 S. Grimme, J. Antony, S. Ehrlich and H. Krieg, *J. Chem. Phys.*, 2010, **132**, 154104.